

This is a repository copy of *Plasma-Enhanced Pulsed Laser Deposition of copper oxide and zinc oxide thin films*.

White Rose Research Online URL for this paper:

<https://eprints.whiterose.ac.uk/id/eprint/161503/>

Version: Accepted Version

Article:

Rajendiran, Sudha, Meehan, David and Wagenaars, Erik orcid.org/0000-0002-5493-3434 (2020) Plasma-Enhanced Pulsed Laser Deposition of copper oxide and zinc oxide thin films. RSC Advances. 065323. ISSN: 2046-2069

<https://doi.org/10.1063/5.0008938>

Reuse

This article is distributed under the terms of the Creative Commons Attribution (CC BY) licence. This licence allows you to distribute, remix, tweak, and build upon the work, even commercially, as long as you credit the authors for the original work. More information and the full terms of the licence here:

<https://creativecommons.org/licenses/>

Takedown

If you consider content in White Rose Research Online to be in breach of UK law, please notify us by emailing eprints@whiterose.ac.uk including the URL of the record and the reason for the withdrawal request.

Plasma-Enhanced Pulsed Laser Deposition of copper oxide and zinc oxide thin films

S. Rajendiran,¹ D. Meehan,¹ and E. Wagenaars^{1, a)}

¹*York Plasma Institute, Department of Physics, University of York, York, YO10 5DD, UK*

(Dated: 3 June 2020)

Plasma-Enhanced Pulsed Laser Deposition (PE-PLD) is a technique for depositing metal oxide thin films that combines traditional PLD of metals with a low-temperature oxygen background plasma. This proof-of-concept study shows that PE-PLD can deposit copper oxide and zinc oxide films of similar properties to ones deposited using traditional PLD, without the need for substrate heating. Varying the pressure of the background plasma changed the stoichiometry and structure of the films. Stoichiometric copper oxide and zinc oxide films were deposited at a pressure of 13 and 7.5 Pa respectively. The deposition rate was approximately 5 nm/min and the films were polycrystalline with a crystal size in the range of 3 - 15 nm. The dominant phase for ZnO was (110) and for CuO they were (020) and (11 $\bar{1}$), where (020) is known as a high-density phase not commonly seen in PLD films. The resistivity of the CuO film was $0.76 \pm 0.05 \Omega \text{ cm}$, in line with films produced using traditional PLD. Since PE-PLD does not use substrate heating or post-annealing, and the temperature of the oxygen background plasma is low, deposition of films on heat-sensitive materials such as plastics is possible. Stoichiometric, amorphous zinc oxide and copper oxide films were deposited on polyethylene (PE) and polytetrafluoroethylene (PFTE).

^{a)}Electronic mail: erik.wagenaars@york.ac.uk

I. INTRODUCTION

Pulsed Laser Deposition (PLD) is a well-established and widely used deposition technique for e.g. dielectric, ferroelectric and magnetic oxide thin films. In particular, metal-oxide wide-bandgap group II-VI semiconductors are widely studied^{1,2}. One of the main advantages of PLD as a deposition technique is the ability to achieve stoichiometric transfer of material from target to substrate. However, in practice, for metal oxides a background atmosphere of oxygen gas is often needed to avoid oxygen-deficient films that are formed under vacuum conditions^{3,4}. In addition, the targets required are of the same complexity as the desired film, making the manufacturing of targets more demanding, compared to pure metal targets. Finally, like many other deposition techniques, PLD often requires elevated substrate temperatures, or post-annealing processes, to achieve high-quality films^{3,5}, preventing direct deposition on heat-sensitive substrates like plastics.

In this paper, a proof-of-concept study for a modified version of PLD, Plasma-Enhanced PLD (PE-PLD)⁶, is presented, which aims to overcome some of the limitations of standard PLD, i.e. the need for multi-element targets and elevated substrate temperatures, for deposition metal-oxide films. The main idea is to combine a standard PLD set up using a metal target with an electrically-produced low-temperature background oxygen plasma. In this way, the sources for metal and oxygen in the deposited film are separated, similar to the approach taken in reactive magnetron sputtering techniques⁷. Our previous modelling investigations indicate that metal atom densities in the order of $10^{14} - 10^{15} \text{ cm}^{-3}$ can be expected in the plasma plume in front of a substrate a few centimeters from the target⁶. In addition, a low-pressure rf-driven Inductively Coupled Plasma (ICP) used as the background plasma can provide reactive oxygen species, e.g. O and O_2^* , at densities of approximately $10^{14} - 10^{15} \text{ cm}^{-3}$, depending on operating conditions⁶. Since these densities are similar, it seems feasible that significant interaction between the plasma plume and background plasma is possible, resulting in deposition of both metal and oxygen at comparable rates. Preliminary investigations of very thin films, 25-50 nm, deposited onto quartz and analysed with Medium Energy Ion Scattering showed broadly stoichiometric films for ZnO and Cu_2O ⁸, but no further characterisation of the film properties was done, nor any variation of deposition parameters. In addition, the oxygen plasma not only provides the oxygen atoms for the thin film, it also provides (chemical) energy to the substrate to assist the growth of the film without additional heating of the substrate. Importantly, the oxygen plasma is a non-equilibrium, pulsed plasma to ensure that its temperature remains low⁹, eliminating significant conductive heating of the substrate

from the plasma, potentially allowing deposition of films onto sensitive substrates. The current paper aims to provide a more comprehensive proof-of-concept for PE-PLD of copper oxide and zinc oxide films, focusing not only on stoichiometry, but also on film structure, morphology and film resistance. In addition, a small range of substrate materials was investigated, in particular heat-sensitive materials.

The combination of a standard PLD plume with a secondary plasma has been reported in literature before. Notably, Dinescu *et al.*, developed a plasma beam assisted PLD system in which a Zn target was ablated in standard PLD, with an additional oxygen plasma beam source also impinging on the substrate, creating ZnO films^{10,11}. The oxygen plasma beam was generated in a separate chamber, with a beam of plasma flowing from this chamber onto the substrate, where this afterglow oxygen plasma interacted with the PLD plume and the growing film on the substrate. With this system, in combination with substrate heating to 800 K, they achieved high-quality ZnO films. Basillais *et al.* followed a similar approach for the deposition of AlN films^{12,13}. A pure Al target was ablated by a laser, while a nitrogen plasma was created in a separate chamber after which it flowed into the ablation chamber, interacted with the metal plasma plume and thin film growth was achieved on heated substrates.

In our work, a similar approach is followed for separating the source of metal and oxygen to deposit metal oxide films, however in our work no substrate heating is applied. The idea is that by using an active plasma that is in direct contact with the ablation plume, instead of an afterglow plasma beam, more reactive and energetic plasma particles impinge to the substrate. The higher energy of these particles, compared to an afterglow plasma or a neutral background gas, means that the diffusion length of these species is longer, resulting in more crystalline films¹⁴. In other words, the energy needed for good surface diffusion is provided by the background plasma rather than the heated substrate. In addition, the background plasma provides particles to the substrate for a much longer time than a laser-produced plasma plume. Tricot *et al.* showed that when using a pulsed-electron beam deposition system, plasma species are being delivered to the substrate for times much longer than in conventional PLD, resulting in polycrystalline films deposited at room temperature, since the probability for an incoming particle to find a good site on the surface for crystalline growth is increased¹⁵. In our case, it is only the oxygen species that are delivered over a much longer time scale, but nevertheless, it can be anticipated that this can promote (poly)crystalline growth.

Huang *et al.*, report ZnO films deposited at room temperature with their RF-PEPLD system¹⁶

and De Giacomo *et al.*, investigated TiO₂ films produced by Plasma-Assisted PLD¹⁷. The layout of both these systems was very similar to ours, however, for both studies, the target was a metal oxide, not a pure metal as in our case. The reason is that the main focus of their work was to reduce droplets in the PLD plume by using a plasma background, not use the background plasma to supply the oxygen for the film. They both showed that droplet contamination is reduced by the plasma, but at the same time, the PLD plume was still capable of depositing high-quality films. Investigations with the aim of room-temperature deposition of metal oxide films from a metal target have not been reported to our knowledge.

The materials chosen for our proof-of-concept study are copper oxide and zinc oxide. There are two common forms of copper oxide: cuprous oxide (Cu₂O) and cupric oxide (CuO). Both are p-type semiconductors with a bandgap of 1.9 – 2.1 and 2.1 – 2.6 eV respectively¹⁸. Cu₂O films are mainly investigated for applications in thin-film transistors (TFTs)¹⁸ and solar cells¹⁹. CuO thin films find applications in gas sensors²⁰ and supercapacitors²¹. One of the main issues in this field is often the poor quality of the films and the high substrate temperatures that are needed for deposition. In addition, controlling the stoichiometry and obtaining single phase CuO or Cu₂O has proven to be challenging¹⁸.

Zinc oxide, ZnO, is an n-type wide-bandgap semiconductor with a direct bandgap of approximately 3.3 eV that finds applications in electronic displays, thin film transistors and solar cells^{22–25}. Background oxygen gas pressure is known to play a crucial role in determining the surface, optical and electrical properties of the resulting films, with the optimum pressure often being different for different types of properties²².

In this paper, a proof-of-concept study for PE-PLD of copper oxide and zinc oxide films is presented. The experimental system making the films is a combination of a standard PLD setup with a pulsed Inductively Coupled Plasma (ICP). The deposited films are characterised using Scanning Electron Microscopy (SEM), Tunneling Electron Microscopy (TEM), Selected Area Electron Diffraction (SAED), Energy Dispersive X-ray spectroscopy (EDX), X-ray Diffraction (XRD) and four-point probe resistivity measurements.

II. EXPERIMENTAL ARRANGEMENT FOR PE-PLD

Fig. 1 presents a schematic diagram of the PE-PLD set up. It consists of a standard PLD set-up positioned inside a low-temperature, low-pressure ICP. The laser is a frequency-doubled,

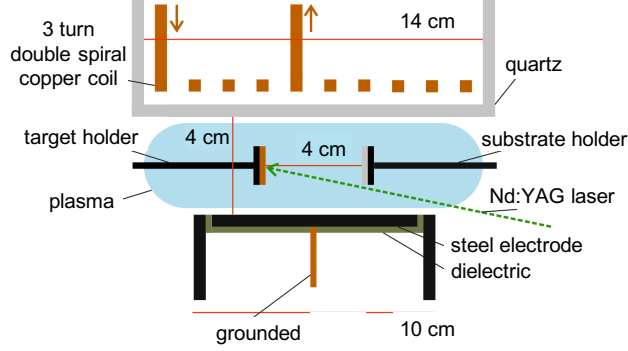


FIG. 1. Schematic diagram of the PE-PLD setup. A standard PLD arrangement is positioned inside a low-pressure Inductively Coupled Plasma (GEC Reference Cell). The whole setup is inside a vacuum chamber (not shown in the diagram).

Q-switched Nd:YAG laser (Continuum Minilite II), operating at 532 nm, with a 5 ns pulse duration, 25 mJ pulse energy and 10 Hz repetition rate. A wavelength of 532 nm, instead of the commonly used UV wavelengths of 355 or 266 nm, was chosen due to the limited laser pulse energy available to ensure sufficient fluence onto the target for significant ablation of material. A 500 mm focal length quartz lens focuses the beam onto the rotatable Cu or Zn target (99.9% purity, Testbourne Ltd.) inside the vacuum chamber. The laser impinges the target under an angle of 45° to the normal and the laser fluence on the target is $9.4 \pm 0.5 \text{ J cm}^{-2}$. A substrate is mounted parallel to the target, at a distance of 40 mm, enough to allow sufficient plume expansion to achieve homogeneous films across the 15 mm diameter substrate area. All analysis of the deposited films was done on the central 10 mm diameter area. The substrate holder is water-cooled to 293 K. The substrate temperature was not measured directly, though the temperature of the substrate holder was monitored with a thermocouple, measuring temperatures below 300 K for all deposition conditions. Quartz is used as a substrate material for most films, apart from the films for XRD analysis of ZnO where crystalline Si (100) wafer was used and the dedicated investigations of deposition of films on plastics, where polyethylene (PE) and polytetrafluoroethylene (PFTE) films were used. The low-temperature ICP that is used is the inductive version of the GEC reference cell²⁶, a standardised source widely used and characterised in the low-temperature plasma community. It consists of a 3-turn double-spiral copper coil, behind a 25.4 mm thick quartz window. The bottom electrode is made of stainless steel and has a diameter of 100 mm. The distance between the quartz window and the bottom electrode is 40 mm, with the target and substrate positioned in the middle between the electrode and the quartz window, about 20 mm from the chamber

central axis. The RF power is applied to the central connection of the coil, with the opposite end of the coil grounded. The driving frequency was 13.56 MHz and an L-type matching network was used for matching the effective load impedance to the RF generator impedance of 50 Ω . The ICP is operated in H-mode at pressures between 4 and 25 Pa and a power of 500 W. To limit the gas temperature in the ICP, it is operated in pulsed mode, with a duty cycle of 10% and repetition rate of 10 Hz to match the laser repetition rate. The ICP plasma pulse is synchronised with the laser using a digital delay generator (Stanford Research Systems DG 535). The laser is set to fire 8 ms after the start of each plasma pulse. Deposition time was 60 minutes, i.e. 3.6×10^4 laser shots, unless stated otherwise. This resulted in film thicknesses of around 200 - 300 nm, depending on ICP pressure. No substrate heating or post-annealing was carried out.

III. RESULTS AND DISCUSSION

A. Stoichiometry

The stoichiometry of films deposited with the PE-PLD experimental system was investigated as a function of oxygen ICP pressure. Since all the oxygen in the resulting films comes from the ICP, it is likely that ICP pressure is the most sensitive control parameter for stoichiometry. Copper oxide thin films were deposited on quartz substrates, from a copper target in an oxygen ICP background, for oxygen pressures ranging from 4 to 25 Pa. Zinc oxide thin films were deposited on quartz substrates, from a zinc target with ICP oxygen pressures between 7.5 and 13.5 Pa. The pressure range for copper oxide was chosen to be wider than zinc oxide since more stoichiometry variation is expected in copper which has two common forms, CuO and Cu₂O, while zinc oxide only has one, ZnO. For the EDX analysis (JEOL 7800F Prime), the electron beam energy (5 keV) was chosen such that no signal from the Si in the substrate was recorded, ensuring that only the deposited films were measured. The estimated range of penetration of the electrons was in the order of 100 nm²⁷, while the deposited films had a thickness in the range of 200 - 300 nm (estimated with a spectral reflectance measurement device, Filmetrics F20). EDX measurements were performed across different positions of the central 10 mm diameter area of the deposited films. No significant variations in the composition were observed for any of the films.

Figs. 2 and 3 show the elemental compositions of the copper oxide and zinc oxide films, respectively, measured by EDX. For copper oxide, it is clear that the overall stoichiometry is influenced

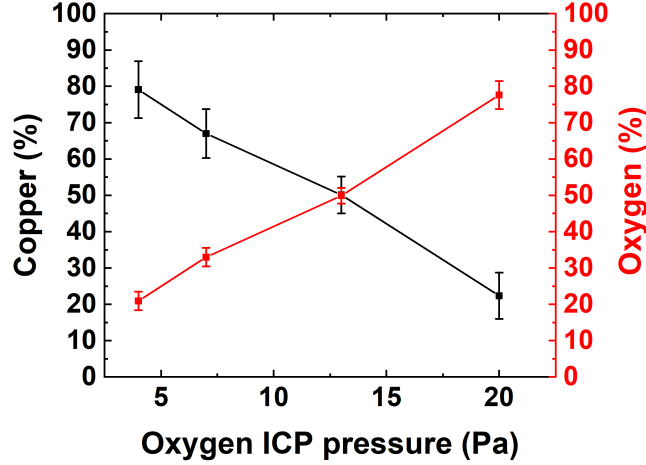


FIG. 2. Elemental composition, in atomic percentages, determined with EDX analysis, of copper-oxide films deposited by PE-PLD for different O_2 pressures of the ICP.

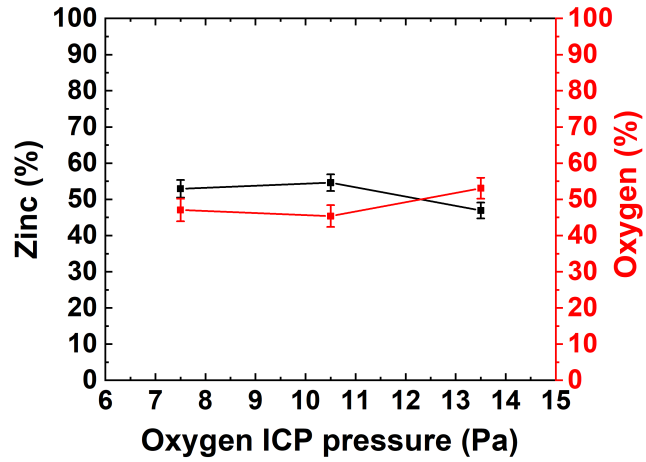


FIG. 3. Elemental composition, in atomic percentages, determined with EDX analysis, of zinc-oxide films deposited by PE-PLD for different O_2 pressures of the ICP.

by the oxygen pressure in the ICP, with higher pressures yielding more oxygen-rich films, most likely due to a higher density of reactive oxygen species. The range of tuning is relatively large; from 80:20 Cu to O to 22:78 over a limited pressure range of 4 – 20 Pa. Importantly, at 13 Pa the stoichiometry is 50:50, matching CuO. Subsequent investigations mainly focus on CuO and therefore were mostly conducted using 13 Pa oxygen pressure in the ICP.

For zinc oxide, see Fig. 3, the stoichiometry is relatively insensitive to the oxygen pressure in the ICP. For pressures 7.5 and 10.5 Pa, the films are slightly oxygen deficient (53:47 and 56:44 metal to oxygen ratio, respectively), while for 13.5 Pa, the film is oxygen-rich at 47:53 metal to

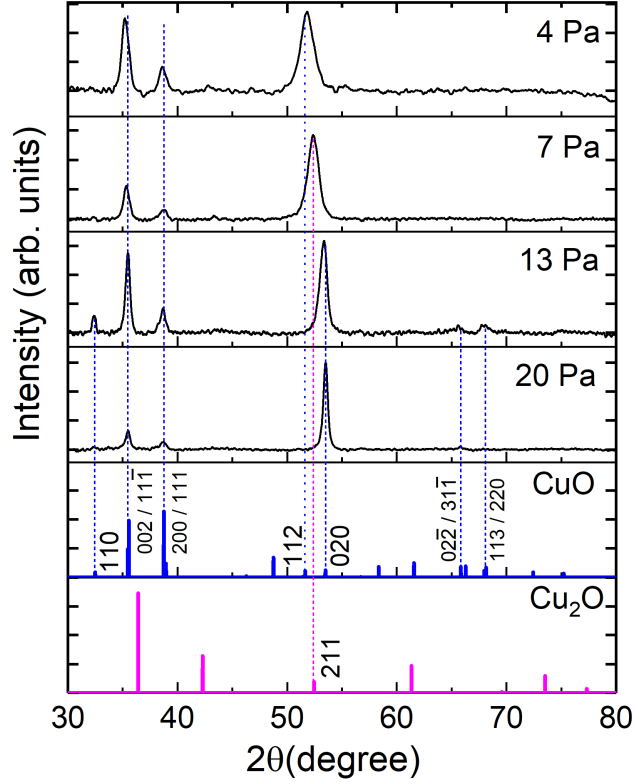


FIG. 4. XRD patterns of copper oxide films deposited on a quartz substrate with PE-PLD for ICP oxygen pressures in the range 4 - 20 Pa. Bottom two frames show reference peaks from ICDD data files 00-045-0937 for CuO and 00-005-0667 for Cu₂O used for peak identification²⁸.

oxygen ratio. The limited range of stoichiometries is most likely due to the fact that there is only one form of zinc oxide (ZnO), while there are two possibilities for copper oxide, CuO and Cu₂O.

The EDX results show that for both CuO and ZnO it is possible to deposit stoichiometric films from pure metal targets using the PE-PLD technique.

B. Structural characterisation of films

In order to determine the crystal structure of the copper oxide and zinc oxide films described in the previous section, XRD (Rigaku Smart Lab, $\lambda = 1.54 \text{ \AA}$) was performed. Fig. 4 shows the measured XRD spectra for the copper oxide films, as a function of ICP pressure, deposited on quartz. The signal intensity was not normalised to film thickness. The observed peaks were identified using the ICDD 00-045-0937²⁸ reference data for CuO and 00-005-0667²⁸ for Cu₂O.

For all pressures, peaks at 35.5° and 38.7° are observed. These peaks correspond to CuO phases,

mainly (11 $\bar{1}$) with a contribution from (002) and (111) with a possible smaller contribution of (200), respectively. For 13 Pa, additional CuO peaks are observed at 32.4°, corresponding to the (110) phase, at 65.7°, corresponding to a combination of (02 $\bar{2}$) and (31 $\bar{1}$) and 68.2°, corresponding to a combination of (113) and (220) phases. Finally, peaks in the region 51- 54° are observed for all pressures; 53.5° at 20 Pa, 53.4° at 13 Pa, 52.4° at 7 Pa and 51.8° at 4 Pa. These peaks can be identified at the CuO (020) phase for 20 and 13 Pa, the Cu₂O (211) phase for 7 Pa and CuO (112) phase for 4 Pa.

It is clear that all of the thin films are polycrystalline, mostly CuO, which is in line with standard PLD based techniques, where it is well documented that deposited films are often polycrystalline due to the non-epitaxial nature of the deposition on quartz substrates²⁹. For 13 Pa, observing only CuO phases is in line with the stoichiometry results from EDX (Fig. 2), giving some confidence that this film is indeed polycrystalline CuO. For 20 Pa, the measured composition suggests a Cu₂O film, however the XRD results show a combination of CuO and Cu₂O structures. The presence of CuO crystals also suggests that in the remainder of this film there must be an abundance of Cu in order for the overall stoichiometry to be 2:1 Cu to O. Finally, for both 4 and 20 Pa, there are some parts of the film that are polycrystalline CuO, however, based on the EDX measurements in Fig. 2, there has to be additional Cu (for 4 Pa) and O (for 20 Pa) in the remainder of the film. Therefore, the film deposited at an ICP pressure of 13 Pa seems to be the most promising in that both the stoichiometry as well as the structure are (polycrystalline) CuO. In addition, a few of the strong observed phases, e.g. the (020) phase, are known to be known high density phases, with high surface energies. These are not commonly observed with other deposition techniques, indicating that there might be significant energy transferred from the ICP to the substrate during the deposition process to allow these high-energy phases to be formed.

Fig. 5 shows an XRD spectrum of the zinc oxide film deposited on Si (100) wafer with the ICP operated at 7.5 Pa. ZnO deposition on Si instead of quartz was chosen to avoid overlap of the broad SiO₂ peak around 20° with the weak ZnO peaks in the range 30 – 35°. Instead, the spectrum in Fig. 5 shows a substrate peak of Si (100) at 69.9°, away from the ZnO peaks at lower angles. The observed ZnO peaks were identified using the COD 2300112³⁰ reference data for ZnO.

The peaks in Fig. 5 at 31.6°, 32.4° and 36.2° correspond to the (100), (002) and (101) phases of ZnO, respectively. The dominant ZnO peak in the spectrum, however, is at 56.3° corresponding to the (110) phase. The observed peaks indicate the film is polycrystalline and has a wurtzite ZnO structure. Variation, or optimisation, of the film structure with operational parameters was not

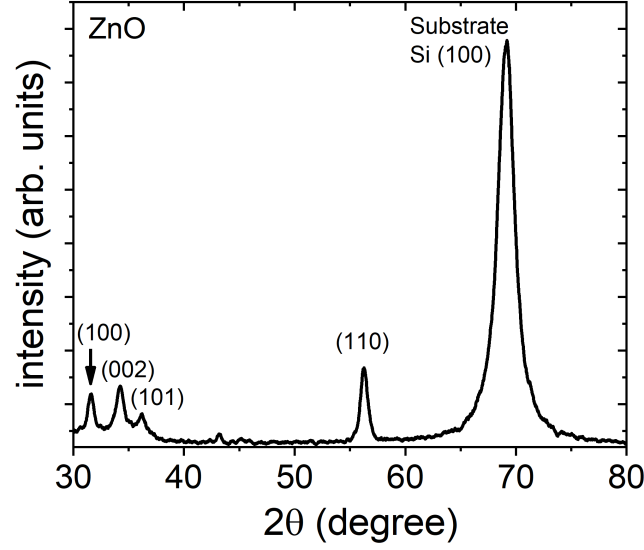


FIG. 5. XRD pattern of ZnO film deposited on a Si (100) substrate with PE-PLD for 7.5 Pa ICP oxygen pressure. Peaks identified with COD data file 2300112³⁰.

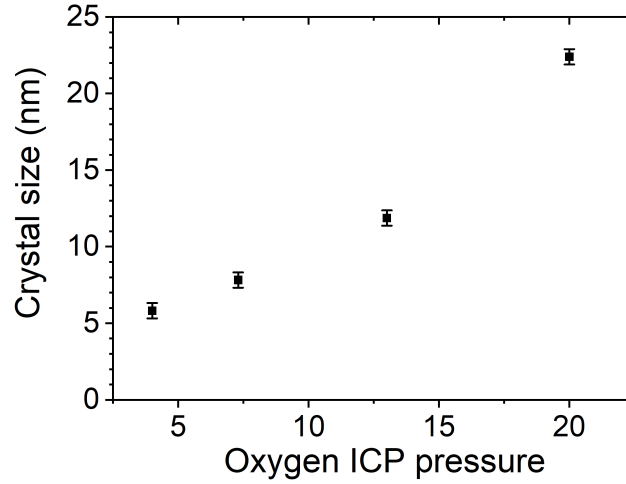


FIG. 6. Crystal size of copper oxide films for different ICP pressure, derived from the (002) peak in the XRD spectra using the Scherrer method³¹.

performed, since this was outside the scope of this proof-of-concept study.

The crystal size of the deposited films can be estimated from the width of the measured XRD peaks using the Scherrer method³¹. A crystal size for the ZnO film of 3.1 ± 0.5 nm was found using the (002) peak. For the copper oxide films, the crystal size was determined from the dominant (020) peak. The results are shown in Fig. 6 and it can be seen that the crystal size increases with ICP pressure, from 5.8 to 22.4 ± 0.5 nm. These crystal sizes are in line with typical values for

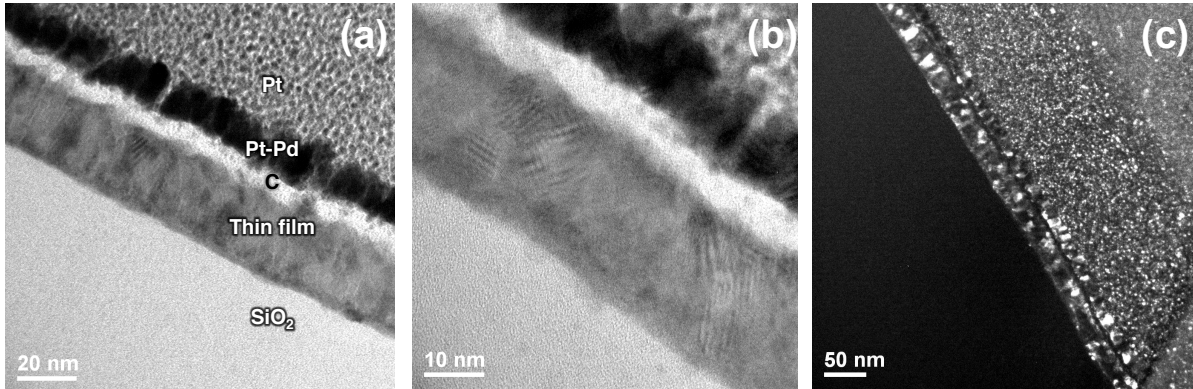


FIG. 7. TEM images of the CuO deposited thin film on a SiO_2 substrate. Fig. (a) shows the sample structure, consisting of the SiO_2 substrate, CuO thin film and the C, Pt-Pd and Pt protective layers. Fig. (b) shows a high-magnification image of the sample, focussing on the thin film and film-substrate interface. Fig. (c) is a dark-field image highlighting the grain structure in the film.

standard PLD-deposited films^{32,33}. The increase of crystal size with background pressure has been reported before for metal-oxide thin films^{34,35} and can be explained by the increased interaction of the metal plume with the background plasma for increasing pressure. This leads to on average larger clusters to be formed before deposition on the surface, eventually leading to larger crystal size in the deposited film³⁵.

For further investigation of the PE-PLD-deposited CuO film at 13 Pa, TEM (JEOL 2010) analysis was undertaken. For this investigation, a thinner film of about 25 nm was deposited using the same operating conditions, but a reduced deposition time of 5 minutes, instead of 60 minutes. An ICP pressure of 13 Pa was chosen since this seemed to have the best stoichiometry and crystal structure. In preparation for the TEM analysis, protective layers of C, Pt-Pd and Pt were deposited onto the CuO thin film. Using a Focused Ion Beam (FEI Nova Nanolab), a section of roughly 15 by 1 μm was milled out and removed from the film. This was then mounted and thinned to approximately 230 nm for TEM analysis. Fig. 7 presents images from TEM analysis of this sample. Fig 7(a) shows an overview of the sample, indicating the quartz substrate, CuO thin film and the three protective layers. It also gives an indication of the homogeneity of the film thickness. Fig. 7(b) presents a high magnification view showing Moiré fringes in the film due to overlapping grains and a nucleation layer of about 3 nm between the quartz substrate and the CuO film. Finally, Fig 7(c) is a dark-field image highlighting the circular shape of the grains in the film. The grain size can be estimated as approximately 10-15 nm, which is in agreement with the 12 nm grain size that

TABLE I. SAED analysis of the CuO deposited thin film on a SiO₂ substrate. The ring number corresponds to the numbers in Figure 8. Identification of diffraction rings is done with ICDD data files 00-045-0937 for CuO and 00-005-0667 for Cu₂O²⁸.

ring number	ring radius (nm ⁻¹)	d spacing (Å)	identified phase
1	3.58	2.79	CuO (110)
2	3.96	2.53	CuO (11 $\bar{1}$) / CuO (002)
3	4.21	2.37	CuO (111) / CuO (200)
4	4.61	2.17	Cu ₂ O (200)
5	5.38	1.86	CuO (20 $\bar{2}$)
6	6.50	1.54	CuO (11 $\bar{3}$) / CuO (202)
7	7.08	1.41	CuO (31 $\bar{1}$) / CuO (02 $\bar{2}$)
8	7.74	1.29	CuO (004) / CuO (22 $\bar{2}$)
9	8.61	1.16	CuO (222)

was derived from the XRD analysis (Fig. 6). In addition, the thickness of the film measured with the TEM was 26 nm, which means the average deposition rate was 5.2 ± 0.5 nm/min, in line with what was measured for the thicker films (60 minute deposition time) using a spectral reflectance measurement device.

The sample structure was investigated with Selected Area Electron Diffraction (SAED), presented in Fig. 8. A circular selected area of 138 nm diameter was investigated, indicated in Fig. 8(a), consisting of the quartz substrate and part of the thin film, approximately 100 nm wide and 20 nm thick. The diffraction pattern in Fig. 8(b) shows a polycrystalline structure. Some of the more dominant diffraction rings are indicated in the figure, details of which can be found in Table I. Most of the observed phases are consistent with the XRD analysis of a thicker film deposited under the same conditions (apart from deposition time). However, the SAED analysis does not show any CuO (020) phase (d spacing of 1.712 Å) which was a dominant phase in the XRD analysis. In addition, there is a Cu₂O (200) phase observed in the SAED analysis which is not present in the XRD analysis. The differences are most likely due to the fact that the films are not exactly the same (different thicknesses) and the measured area is much smaller in the case of SAED (order 100 nm diameter) compared to XRD (order 10 mm diameter). This suggests that there could be

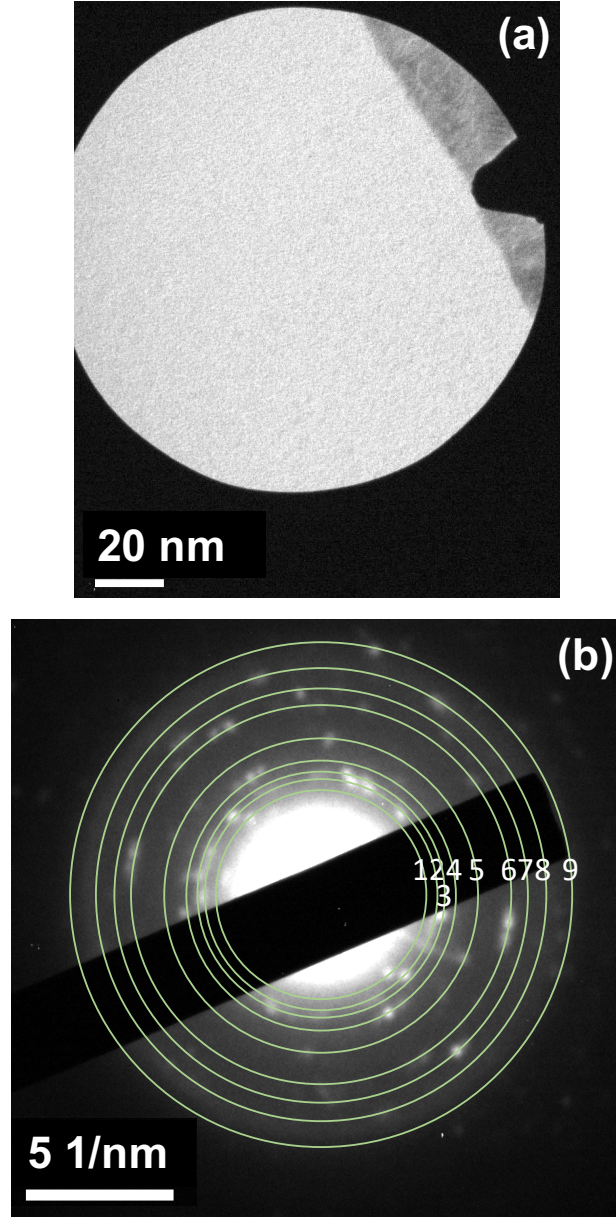


FIG. 8. (a) Selected Area Aperture for SAED. The bulk of the image is the quartz substrate with the thin film, approximately 20 nm thick, in the top right corner. b) SAED image of the CuO deposited thin film on a SiO₂ substrate. Selected diffraction rings are indicated on the image, details can be found in Table I.

local variations in the structure of the film which is not unlikely given the many different phases that are present in these polycrystalline films. Also, the composition is heavily dominated by CuO phases, but there is some evidence that there are also some Cu₂O grains present in the film.

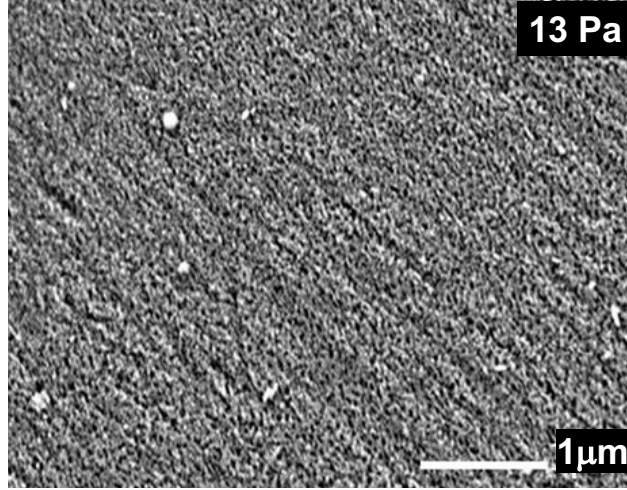


FIG. 9. SEM image of the CuO deposited thin film on the SiO₂ substrate.

C. Surface morphology and film resistance

Fig. 9 presents an SEM image of the PE-PLD-deposited CuO film. It shows a relatively smooth surface. There is some evidence for a few particulates with a maximum size of about 100-200 nm. However, no micron-size particulates were observed in any of the films, a known issue with standard PLD, indicating that the background plasma (or gas) is capable of preventing any particulates reaching the substrate.

Finally, resistance of the film (60 minute deposition time) was measured using a four point probe. A resistance of $0.76 \pm 0.05 \Omega \text{ cm}$ was found which is in line with literature values in the range of 0.01 - 1 $\Omega \text{ cm}$ for CuO thin films³⁶.

D. Thin film deposition on plastic substrates

Since the substrate temperature is kept low, close to ambient temperature, deposition of thin films on heat-sensitive substrates such as plastics should be possible with PE-PLD. As a proof-of-concept, zinc oxide and copper oxide films were deposited onto PE and PTFE film substrates. The deposition conditions were 7.5 Pa O₂ ICP pressure, 500 W RF power and 60 minutes deposition time for both the zinc and copper cases. EDX analysis shows, within error, stoichiometric ZnO films, with a composition of 51:49 and 52:48 zinc to oxygen for PE and PTFE substrates, respectively. For the copper oxide samples the stoichiometry was 67:33 and 68:32 copper to oxygen for PE and PTFE substrates, respectively. The error on all EDX measurements was ± 2 atomic%. This

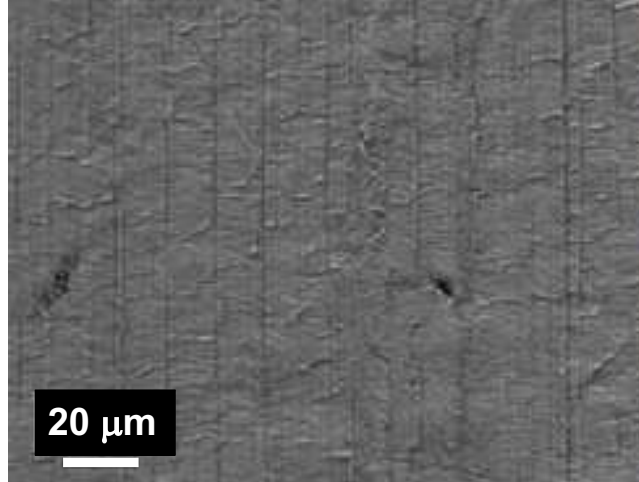


FIG. 10. SEM image of the copper oxide film deposited on PE at 7.5 Pa O_2 pressure and with 500 W RF power in the ICP. Deposition time was 60 minutes. The vertical ridges on the film in the SEM image originate from the PE substrate, not the copper oxide film.

suggests the copper oxide film is Cu_2O as was the case for the samples deposited on quartz at this pressure (Fig. 2). XRD analysis showed no metal-oxide peaks for any of the films, suggesting that they are all amorphous.

Fig. 10 shows an SEM image of the copper oxide film on a PE substrate. The film appears homogeneous without any micron-sized particulates. The vertical ridges that can be seen originate from the structure of the PE substrate and are not a result of the film deposition process. The adhesion of the films onto the substrates was not investigated in any detail. However, it was not possible to remove the films by bending and flexing the substrates after deposition, suggesting some reasonable adhesion properties. Of course, this is only a preliminary investigation and more detailed characterisation of the adhesion properties will need to be performed in the future to allow use of these films in applications and devices.

IV. CONCLUSIONS

PE-PLD with a pure metal target and a background low-temperature oxygen plasma (ICP) can successfully be used to deposit copper oxide and zinc oxide thin films on a quartz substrate without external substrate heating or post-annealing. The films were polycrystalline and the stoichiometry of the copper oxide films could be tuned by varying the ICP pressure. Many of the characteristics of the deposition technique and resulting films are similar to standard PLD using metal oxide

targets and substrate heating, e.g. similar crystal size and deposition rate^{29,37,38}. The resistivity of the film was also in line with what is reported for PLD-deposited films. Deposition of amorphous, stoichiometric zinc oxide and copper oxide films onto sheets of PE and PTFE was shown to be possible with PE-PLD. In conclusion, PE-PLD is capable of depositing films similar to PLD in stoichiometry and crystallinity but using pure metal targets instead of metal oxide ones and without substrate heating. Future investigations into performance of PE-PLD-deposited films in application-focused devices is needed to ensure PE-PLD can indeed produce the same, or better, quality films as conventional PLD.

ACKNOWLEDGMENTS

The authors would like to thank Jon Barnard, Leonardo Lari and Kevin O’Grady for their assistance with the TEM, SAED, SEM and XRD measurements. We also acknowledge financial support from the UKRI Engineering and Physical Sciences Research Council (EPSRC), grant EP/K018388/1. The data that support the findings of this study are available from the corresponding author upon reasonable request.

REFERENCES

- ¹R. Eason, *Pulsed Laser Deposition of Thin Films - Applications-Led Growth of Functional Materials* (Wiley-Interscience, Hoboken, NJ, 2007).
- ²J. A. Greer, J. Phys D: Appl. Phys. **47**, 034005 (2014).
- ³H. Christen and G. Eres, J. Phys: Condens. Matter **20**, 264005 (2008).
- ⁴Z. Marton, S. S. A. Seo, T. Egami, and H. N. Lee, J. Crystal Growth **312**, 2923 (2010).
- ⁵A. Singh and R. Mehra, J. Appl. Phys. **90**, 5661 (2001).
- ⁶S. Rajendiran, A. K. Rossall, A. Gibson, and E. Wagenaars, Surf. Coat. Technol. **260**, 417 (2014).
- ⁷P. Kelly and R. Arnell, Vacuum **56**, 159 (2000).
- ⁸A. K. Rossall, J. A. van den Berg, D. N. Meehan, S. Rajendiran, and E. Wagenaars, Nuclear Inst. and Methods in Physics Research B **450**, 274–278 (2019).
- ⁹D. N. Meehan, K. Niemi, and E. Wagenaars, Jpn. J. Appl. Phys. **59**, SHHB03 (2020).

- ¹⁰L. C. Nistor, C. Ghica, D. Matei, G. Dinescu, M. Dinescu, and G. V. Tendeloo, *J. Crystal Growth* **277**, 26 (2005).
- ¹¹N. Scarisoreanu, D. G. Matei, G. Dinescu, G. Epurescu, C. Ghica, L. C. Nistor, and M. Dinescu, *Appl. Surf. Sci.* **247**, 518 (2005).
- ¹²A. Basillais, C. Boulmer-Leborgne, J. Mathias, and J. Perrière, *Appl. Surf. Sci.* **186**, 416 (2002).
- ¹³A. Basillais, R. Benzerga¹, H. Sanchez, E. L. Menn, C. Boulmer-Leborgne, and J. Perrière, *Appl. Phys. A* **80**, 851 (2005).
- ¹⁴M. Nistor, N. B. Mandache¹, and J. Perrière, *J. Phys. D: Appl. Phys* **41**, 165205 (2008).
- ¹⁵S. Tricot, C. Boulmer-Leborgne, M. Nistor, E. Millon, and J. Perrière, *J. Phys. D: Appl. Phys* **41**, 175205 (2008).
- ¹⁶S. H. Huang, Y. C. Chou, C. M. Chou, and V. K. S. Hsiao, *Appl. Surf. Sci.* **266**, 194 (2013).
- ¹⁷A. D. Giacomo, V. A. Shakhmatov, G. S. Senesi, and S. Orlando, *Spectrochim. Acta B* **56**, 1459 (2001).
- ¹⁸E. Fortunato, P. Barquinha, and R. Martins, *Adv. Mater.* **24**, 2945 (2012).
- ¹⁹T. K. S. Wong, S. Zhuk, S. Masudy-Panah, and G. K. Dalapati, *Materials* **9**, 271 (2016).
- ²⁰P. Samarasekara, N. T. R. N. Kumara, and N. U. S. Yapa, *J. Phys.: Condens. Matter* **18**, 2417 (2006).
- ²¹S. M. Pawar, J. Kim, A. I. Inamdar, H. Woo, Y. Jo, B. S. Pawar, S. Cho, H. Kim, and H. Im, *Sci. Rep.* **6**, 21310 (2016).
- ²²Ü. Özgür, Y. I. Alivov, C. Liu, A. Teke, M. A. Reshchikov, S. Doğan, V. Avrutin, S.-J. Cho, and H. Morkoç, *J. Appl. Phys.* **98**, 041301 (2005).
- ²³R. Kumar, G. Kumar, O. Al-Dossary, and A. Umar, *Mater. Express* **5**, 3 (2015).
- ²⁴G. Kaur, A. Mitra, and K. L. Yadav, *Prog. Nat. Sci. Mater.* **25**, 12 (2015).
- ²⁵M. Laurenti, S. Porro, C. F. Pirri, C. Ricciardi, and A. Chiolerio, *Crit. Rev. Solid State Mater. Sci.* **42**, 153 (2017).
- ²⁶P. A. Miller, G. A. Hebner, K. E. Greenberg, P. D. Pochan, and B. P. Aragon, *J. Res. Natl. Inst. Stand. Technol.* **100**, 427 (1995).
- ²⁷K. Kanaya and S. Okayama, *J. Phys. D: Appl. Phys.* **5**, 43 (1972).
- ²⁸S. Gates-Rector and T. Blanton, *Powder Diffr.* **34**, 352 (2019).
- ²⁹M. Kawwam, F. Alharbi, A. Aldwayyan, and K. Lebbou, *Appl. Surf. Sci.* **258**, 9949 (2012).
- ³⁰H. Sowa and H. Ahsbahs, *J. Appl. Crystallogr.* **539**, 169 (2006).
- ³¹P. Scherrer, *Göttinger Nachrichten Gesell.* **2**, 98 (1918).

- ³²S. Kitazawa, Y. Choi, S. Yamamoto, and T. Yamaki, *Thin Solid Films* **515**, 1901 (2006).
- ³³S. J. Henley, M. N. R. Ashfold, and D. Cherns, *Surf. Coat. Technol* **177-178**, 271 (2004).
- ³⁴N. R. C. Raju, K. J. Kumar, and A. Subrahmanyam, *J. Phys. D: Appl. Phys.* **42**, 135411 (2009).
- ³⁵A. Kaushal and D. Kaur, *J. Nanopart. Res.* **13**, 2485 (2011).
- ³⁶F. M. Li, R. Waddingham, W. I. Milne, A. J. Flewitt, S. Speakman, J. Dutson, S. Wakeham, and M. Thwaites, *Thin Solid Films* **520**, 1278 (2011).
- ³⁷E. Manikandan, M. K. Moodley, S. S. Ray, B. K. Panigrahi, R. Krishnan, N. Padhy, K. G. M. Nair, and A. K. Tyagi, *J. Nanosci. Nanotechnol.* **10**, 5602 (2010).
- ³⁸M. Anusha, D. Arivuoli, E. Manikandan, and M. Jayachandran, *Opt. Mater.* **47**, 88 (2015).